# ESTIMATING THE WATER BUDGET OF EXTRATROPICAL CYCLONES WITH THE PRECIPITATION EFFICIENCY

---

A Thesis

presented to

the Faculty of the Graduate School

at the University of Missouri-Columbia

---

In Partial Fulfillment

of the Requirements for the Degree

Master of Science

---

By

AMANDA COOLEY

Dr. Patrick Market, Thesis Advisor

MAY 2018

The undersigned, appointed by the dean of the Graduate School, have examined the thesis entitled

ESTIMATING THE WATER BUDGET OF EXTRATROPICAL CYCLONES WITH THE PRECIPITATION EFFICIENCY

presented by Amanda Cooley,

a candidate for the degree of master of science,

and hereby certify that, in their opinion, it is worthy of acceptance.

Professor Patrick Market

Professor Tony Lupo

Professor Benjamin Knapp

## Acknowledgements

I would like to start off by thanking Dr. Patrick Market for advising both my graduate and undergraduate work; and being an amazing mentor and teacher. He has been patient with my work through the struggles of school and maintaining a work balance. Secondly, thank you to all my friends who help take away the stress from homework and projects. Last but not least, I want to thank my parents and family for supporting me through my years of schooling.

## Contents

## Figures

## Tables

## Abstract

Estimating the water budget of three mid-latitude extratropical cyclones is attempted from the perspective of the precipitation efficiency (PE), using a method proposed for the study of convective columns. Using a lagrangian, system-relative volume centered on the surface low pressure, each cyclone was followed for most of its lifetime within a pre-defined volume (7 degrees latitude x 9 degrees longitude, or approximately 700 x 700 km). A comparison is then made of total atmospheric water vapor ingested to total moisture eliminated (as precipitation). We hypothesize that the PE increases with the intensity of the cyclone. This small sample confirms that idea, and thus encourages further study with this approach.

## Chapter 1. Introduction

The ability to anticipate rainfall (or lack thereof) has been an area of study in meteorology for many years. From the beginning of a cyclone's evolution to its decay, the amount of water vapor ingested varies from cyclone to cyclone. Precipitation throughout a cyclone's life cycle is of interest in relation to this behavior in order to understand the precipitation efficiency (PE) of a cyclone. Precipitation efficiency is defined in various works of (e.g., Anip et al. 2006) as the ratio of total precipitation to the total amount of ingested moisture. Early work by Bradbury (1957) took a synoptic view of several mid-latitude cyclones in order to better understand how they process water vapor over their lifetime. Her work examined several different extratropical cyclones to assess changes in their water budgets. The focus of Bradbury (1957) was less about cyclone intensity, and focused primarily on moisture availability and convective columns, with an emphasis on short term water cycling using the precipitation efficiency, and the subsequent risk of flash flooding.

As a function of scale, Bradbury (1957) had established an eulerian volume through which her cyclones moved; whereas Doswell et al. (1996) suggested a lagrangian volume that moved with the convective column in question. At even larger scales, climate concerns have come to the fore more recently, with examinations of long-term changes in moisture availability, and impacts from drought to the enhanced availability of moisture to both tropical and extratropical cyclones (IPCC 2007). Various types of cyclones and intensities hold different water budgets in similar instances.

In the present study, a hybrid of the aforementioned approaches is used. As technology advances and various selections of studies have been conducted in recent meteorology, a modernized approach to study precipitation efficiency of various cyclones is in order. A cyclone

has the capability of tracking over thousands of miles from its immature stage to its decay. Assessing an atmospheric system's water budget cannot be done entirely until that system has completed its lifecycle. For an eulerian method, the best calculation of the cyclone's water budget is done by gathering the inflow and outflow of water vapor within an area around the center of the cyclone as it passes through at a mature stage of its evolution. A grid point area of known location and size can be placed over an area the cyclone travels through. At 3-hour intervals the moisture ratio in and out of the cyclone is used to calculate the precipitation efficiency for each time. The average moisture ratio of each time is used to calculate the precipitation efficiency of the cyclone's lifecycle.

In earlier studies such as Market et al. (2003), cyclones of a convective nature were assessed through a summer term. It is of interest to correlate if wintertime stratiform type systems adhere to the same precipitation efficiency findings. Multiple cyclone cases are acquired through the North American Regional Reanalysis (NARR) for precipitation data at three hour intervals. Cyclone intensities are of key interest in this study; explosive, typical, and non-deepening cyclones are categorized for comparisons of results. Three core cases are used as identifiers for each classification of intensity. Nine other cyclone events are used to enhance sample size and comparisons; three cases for explosive, typical, and non-deepening each. It is hypothesized, as cyclone intensity increases, so will its lifetime precipitation efficiency.

This thesis also uses experimental software scripts for calculating cyclone precipitation efficiency in both the eulerian and lagrangian frameworks.

## Chapter 2. Background

Various studies in meteorology have been conducted for many years pertaining to the precipitation efficiency of different storm systems and types. Before the research of this paper was conducted, an extensive background review of these previous works was done with a goal of understanding the methods of calculating PE, different storm types and their correlation or lack thereof, and seasonal variations.

Early work by Bradbury (1957) studied three different storms with a purpose in comparing them with respect to their convective qualities. Each storm was fed by warm and humid air brought north from the Gulf of Mexico, the first of which displayed thunder, the second with little thunder, and the third with no thunder. Bradbury's (1957) goal was to compare results from values computed by the water vapor balance equation to actual rainfall observations from an area around the center of the cyclone. Bradbury (1957) used an Eulerian method to calculate the PE of each storm. A box is placed over a particular place of interest in the path of the cyclone where the system passes through. Results showed agreement between the calculated values and the actual precipitation amounts with some measures of discrepancy. Possible reasons for these systematic discrepancies found in Bradbury's (1957) studies are due to processes of evaporation. Discrepancies similar to Bradbury's (1957) findings are also found in multiple later studies (e.g., Doswell 1996; Market et al. 2003; Anip and Market 2006). Bradbury (1957) described some of these reasons to be due to possible escape of water vapor out the top of a column or even horizontally as winds create an anvil extending forward from the storm. These processes would tend to create lower rainfall amounts compared to those computed from the water vapor balance equation. In contrast, Bradbury (1957) hypothesized re-evaporation of fallen rain would likely cause higher rainfall amounts. With respect to the storms convective

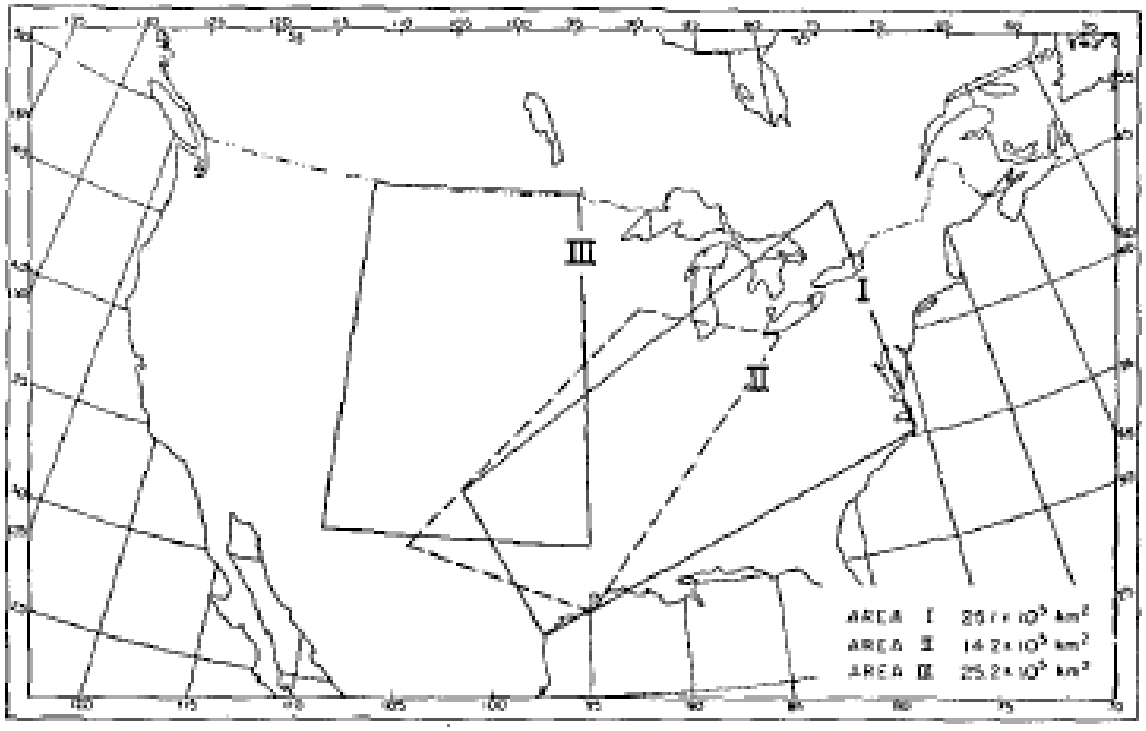


FIG. 1. Horizontal projection of the vertical walls through which the moisture influx was computed. Area I refers to Storm I, Area II to Storm II and Area III to Storm III.

Fig. 2.1. Bradbury's (1957) method for calculating PE using an Eulerian cyclone.

qualities, it was found that maximum rainfall amounts occurred in the areas of the strongest vorticity gradient.

In terms of a more climatological approach to the studies of precipitation efficiency, Sellers (1965) describes ideal locations in both northern and southern hemispheres favorable for precipitation and evaporation. In the United States, the mid-latitudes are known for frequent cyclonic activity resulting in heavy precipitation events. As Sellers (1965) thoughtfully mentions, the amount of water vapor does not necessarily pertain to the amount of precipitation released. This raises the question of how efficient these cyclones are actually at releasing the

amount of precipitation compared to the amount of water vapor these systems actually have. Not only does Sellers (1965) look at geographical locations of PE, it is also noted that PE values are typically lower in summer months versus winter months in the US. This is of key interest in the following research as I am mainly interested in cold month activity.

A study similar to Bradbury (1957), is a case study of an event from 1961 February 17 through February 19 developing near the Texas panhandle and proceeding to the Great Lakes (Rasmussen et al. 1969). In contrast with Bradbury's (1957) work, one of Rasmussen's et al. (1969) goals was to find a precipitation pattern with respect to a moving cyclone. With this type of lagrangian view, the grid point is placed over the center of the cyclone with the horizontal axis pointing towards the direction of movement. The area of interest is reduced to only encompass active precipitation of the storm and is rectangular in shape. Rasmussen's (1969) goal, similar to that of Bradbury's (1957) is to compute the atmospheric water balance of the precipitating area. To encompass the full spectrum of the storm as it moves with time, the data was tabulated in three observation periods: 0000Z and 1200Z, 18 February 1961, and 0000Z, 19 February 1961. Similar to Bradbury's (1957) work, the values computed from the water balance equation correspond fairly well to the rain gauge data (Rasmussen et al. 1969). Calculating the precipitation efficiencies of this storm at the three times established, percentages of 72%, 122%, and 83% were calculated respectively; with the efficiency defined as the ratio of precipitation using the water balance equation over the condensate (Rasmussen et al. 1969). It is important to keep in mind these are 12-hr precipitation efficiencies. It is interesting to see how these will correlate to total storm precipitation efficiency averages.

Unlike we've seen in previous works (eg., Bradbury 1957; Rasmussen et al. 1969) a study of precipitation efficiency testing a broader spectrum of storm classifications is done by

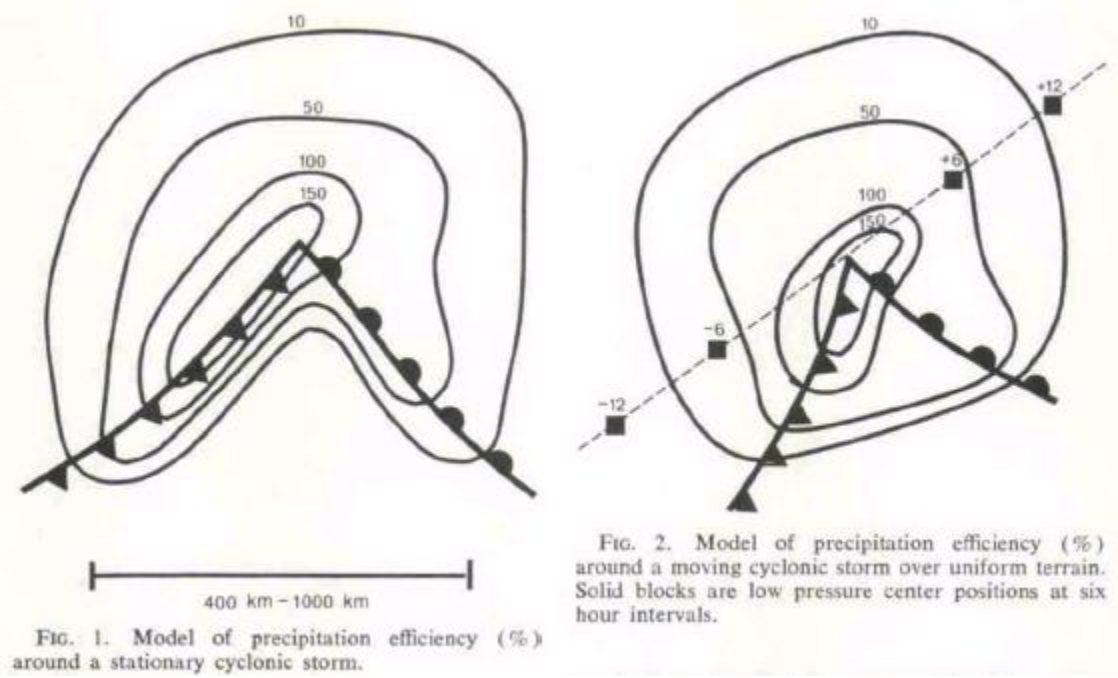


FIG. 1. Model of precipitation efficiency (%) around a stationary cyclonic storm.

FIG. 2. Model of precipitation efficiency (%) around a moving cyclonic storm over uniform terrain. Solid blocks are low pressure center positions at six hour intervals.

Fig. 2.2. Robinson and Lutz's (1978) figure using a Lagrangian method of calculating PE at different time intervals and locations of the lowest central pressure.

Robinson and Lutz (1978). In his analysis, 20 cyclonic storms were analyzed with various sizes, age, intensity, and location in the eastern sector of the United States with goals of producing a model to distribute precipitation efficiencies around a cyclonic storm. This model takes into account different storm parameters such as size, age, speed of movement, and intensity, while estimating effects of topography and advection. During the storms evolution, Robinson and Lutz (1978) calculated the precipitation efficiency at 12 hour increments. Figure 2.2 is an example of the path a cyclone takes and a langrangian method for calculating PE. Using radiosonde data to calculate precipitable water vapor (PWV) from the temperature and humidity values, the PE is calculated with PWV values at 12 hour intervals. Thus, assumptions must be made as to the distribution of PWV within the period. Certain cyclonic properties such as fronts pose a questionable amount of accuracy due to their fast movements. Robinson and Lutz (1978)

assumed PWV was equal on both sides of the front. This gives a 12 hour average of the storm precipitation efficiency. For all 20 storms reviewed in this study, many similarities were found despite the differences mentioned earlier. The areas of the cyclone with the highest PE values tended to focus around frontal regions and within the cold sectors for each type of cyclone. After runs of the model are done on individual storms, Robinson and Lutz (1978) determined it is not best used directly for single cases, but is more ideal in determining seasonal average conditions and climatological predictions.

Similar to many of the other papers already discussed, Doswell et al. (1996) looks at the significance of precipitation efficiency as an ingredient in specifically forecasting for flash flood events. Despite what many may think, flash flooding has become the number three fatal meteorological event (WWS 2017). Advances in tornado warnings and other severe weather have made further progress in the forecasting of fatal events. Difficulties in predicting flash flooding lie in the question of not only will the event happen, but the severity of it (Doswell et al. 1996). Like Sellers (1965) discussed in the climatological approach of precipitation efficiency, it's not as simple as observing how much water vapor is ingested into a cyclone and assuming that is exactly what will precipitate out of the storm. Figure 2.3 gives an interesting visual of the amount of water vapor ingested into a storm in comparison to that which is precipitated out. In essence, this is the definition of precipitation efficiency. Doswell et al. (1996) also discuss this issue and some reasoning behind it. Just like Robinson and Lutz (1978), Doswell et al. (1996) defines precipitation efficiency as the ratio of the mass of water falling as precipitation over the influx of water vapor. Because of the errors that may occur when taking an instantaneous calculation of PE, Doswell et al. (1996) find the most accuracy in calculating over a time average of the cyclone. In the developing stages of a cyclone, PE is likely to be zero or even negative,

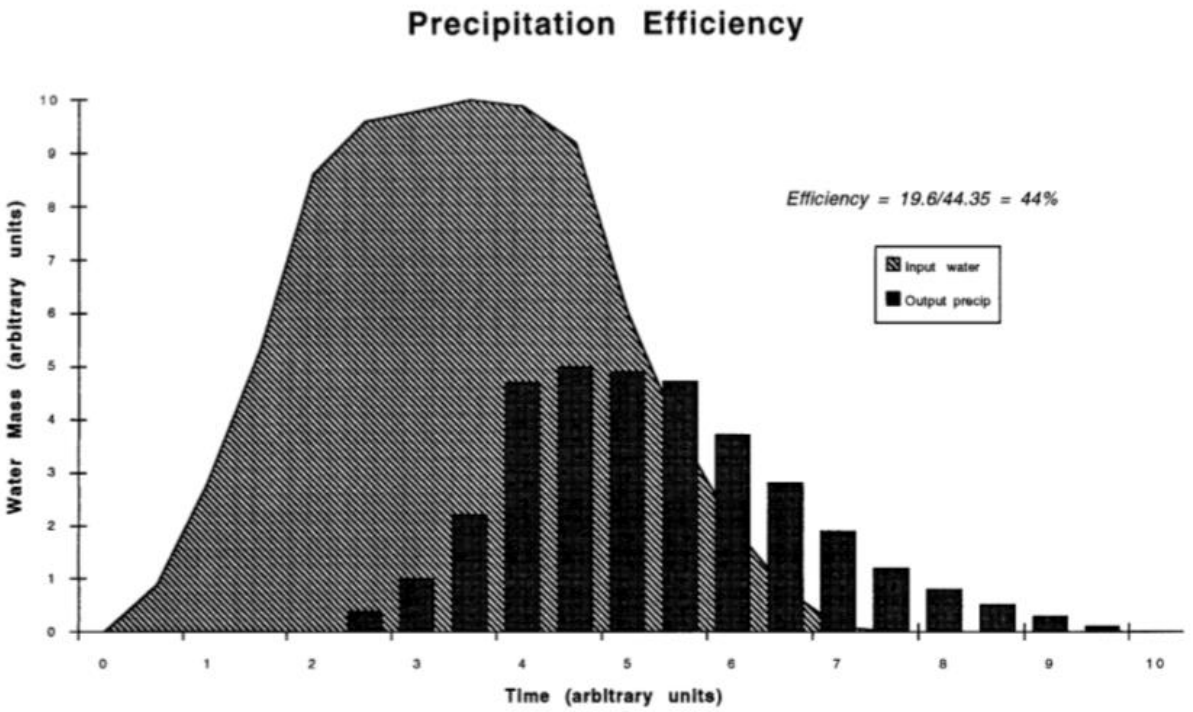


FIG. 1. Schematic illustration of the time variation of water vapor input (cross-hatched area) and the precipitation output (vertical bars) over the lifetime of a precipitation system. The units are arbitrary, so the system being portrayed can be any precipitating process with a developing phase (time = 0–3 units), a mature phase (time = 3–6 units), and a dissipating phase (time = 6–10 units). For this example, the areas under the respective curves give a precipitation efficiency of about 44%.

Fig. 2.3. Doswel's et al. (1996) figure describing the difference of input and output of water vapor.

when water vapor is being ingested into the storm, but precipitation is not yet falling (Doswell et al. 1996). A similar theory is also applicable to the decay of a cyclone. As the storm dies, water vapor is no longer being ingested yet the storm is still precipitating out. In such circumstances, PE may be greater than 100% (Doswell et al. 1996).

All the studies reviewed up to this point (eg., Bradbury 1957; Sellers 1965; Rasmussen et al. 1969; Robinson and Lutz 1978; Doswell et al. 1996) have been focused on cyclones in the United States. Of similar interest in precipitation efficiency is a study done by Rockel and Karstens (2001) of three extratropical cyclones tracking over Europe with water vapor source from the Baltic Sea catchment. In this region, the Baltic Sea provides a main source of ingested

water vapor for developing cyclones. Knowing the PE of these cyclones can help forecast how much rain is to be expected to be beneficial for the community. In order to accurately calculate the PE of a cyclone, Rockel and Karstens (2001) face an issue we've seen previously (eg., Bradbury 1957) for the best way to shape a grid around a cyclone to include/exclude areas of clouds and precipitation versus areas of none. In this case, a circle was chosen with the center being the center of the cyclone where the lowest pressure was recorded, with radii of 500 km covering most of the cyclone while minimizing effects of grid boxes that do not belong in the area of the cyclone (Rockel and Karstens 2001). Between the three storms interestingly, the strongest of the cyclones (largest pressure gradient) produces the least amount of precipitation.

Moving back to the Midwest United States, Market et al. (2003) performed a study of warm season cyclones with a goal of understanding deep moist convection of mesoscale convective systems (MCS) and how to better forecast these in terms of flash flooding with advanced warning up to 6 hours. Data used for this study was acquired from stage-III radar mosaics for the 6 hr total precipitation (Market et al. 2003). With this time spread, the development, maturity, and dissipation of the entire MCS life cycle can be studied. For a precipitation efficiency of the storms, a time average is taken over the whole storm life cycle versus an instantaneous value. To check to accuracy of the radar data, rain gauges were used. Calculating water vapor for the denominator of the PE equation was done with data from the Rapid Update Cycle (RUC) for each hour within the six hour times from radar data (Market et al. 2003). Even with this data available, assumptions still must be made in calculating the precipitation efficiency. Because the RUC was calculated every hour and only 6 hour radar derived precipitation data were available, the precipitable water was divided equally among all 6 hrs. The problem that occurs when this assumption is made is that not every hour within that 6

hour time frame has precipitation occurring. As a result, this tends to decrease the total precipitation in the number of the PE equation, which in turn causes a decrease in PE percentages (Market et al. 2003). Another factor that may affect PE values could be the evaporation of precipitation before it reaches the ground. This is due to a low-level relative humidity; if this is reversed with a higher relative humidity, evaporation would be reduced below the cloud base, increasing PE. Another interesting factor studied by Market et al. (2003), is how convective inhibition affects PE. Convective inhibition is responsible for limiting the vertical motion of a convective column. With this, it makes sense that a lower CIN value would increase PE due to the ability of the column to lift, condense, and aggregate water vapor into precipitation (Market et al. 2003). In contrast to CIN, the bulk shear of a convective system is inversely related to PE because as shear increases, a column becomes less vertically stacked and more angled. This results in more likely dry air entrainment causing a decrease in PE due to higher evaporation of potential precipitation particles (Market et al. 2003). Lastly, Market et al. (2003) takes a look to see if there's any correlation between convective available potential energy (CAPE) and PE and did not find any such positive relationship. With these environmental factors found to have a significant affect in the results of PE, forecasters can use these as tools to better predict how PE can affect different types of storms (Market et al. 2003).

A study of various types of storms was conducted over Columbia, Mo, over a time frame of 1 year to verify any differences in precipitation efficiency of convective versus stratiform type storms (Anip and Market 2006). PE results from these storms ranged from -78% to 236% (Anip and Market 2006). At this point, we've seen many theories given for PE values below 0% and over 100% (eg., Bradbury 1957; Doswell et al. 1996; Market et al. 2003). In terms of instantaneous values of PE, values greater than 100% can be due to the dissipating stage of a

storm where it continues to rain out (Anip and Market 2006). Negative values are possibly due to the advection of moisture through the top of a storms anvil. When calculating the moisture flux convergence, this would create a negative value in the PE equation. With respect to seasonal variations in values of PE, Anip and Market (2006) found that the warm season from March through August tended to be higher than storms in the cold months, from September through February. With this being the case, the warm season is more typical of convective systems, which would make sense they have a higher PE value because of their ability to collect water droplets due to stronger updrafts and downdrafts. During the warm season, cloud depth also tends to be greater, promoting higher levels of moisture for the aggregation of rain drops (Anip and Market 2006).

Taking a look at precipitation efficiency from a modeling perspective, Sui et al. (2007) discusses the importance of PE as a parameter assumption of cumulus parameterization. Sui et al. (2007) defines PE in two different ways; cloud microphysics precipitation efficiency (CMPE) when precipitation is proportional to the condensation rate, and a large-scale precipitation efficiency (LSPE) where precipitation is proportional to the moisture flux in more convective type systems. This study used a two-dimensional cloud-resolving model simulation to verify PE produced during model integration (Sui et al. 2007). Both CMPE and LSPE were found to be able to obtain values over 100% but only LSPE produced any negative percentages.

# Chapter 3. Data and Methods

## 3.1 Data

### 3.1.1 NARR

For the purpose of conducting this research, the data for each cyclone case was acquired from the North American Regional Reanalysis (NARR) dataset. The NARR is defined by the National Centers for Environmental Prediction (NCEP) as "a long-term, dynamically consistent, high-resolution, high frequency, atmospheric and land surface hydrology dataset for the North American domain" (Mesinger et al. 2006). The NARR is valid starting in 1979 to present with continuation currently in near real-time as the Regional Climate Data Assimilation System (RCDAS) (Mesinger et al. 2006). Before development of the NARR, resolution, accuracy, and consistency were lacking in model output predictions. Improvements obtained consist of "direct assimilation of radiances, improved data processing, and several Eta model developments" (Mesinger et al. 2006). Of particular interest to the research of this paper, the NARR was expected to help in the forecasting of extreme weather events such as flash flooding, droughts, and other aspects pertaining to the variability of the water budget (Mesinger et al. 2006). The ability to make such improvements is due to the reformed lateral boundaries and Eta model developments. In particular, the land to surface component of the model is more accurate than any previous model due to a newer version of the NCEP Eta model (Mesinger et al. 2006). This variable is important in atmospheric conditions as it is directly correlated to the hydrological cycle and how land relates to atmospheric interactions (Mesinger et al. 2006).

The NARR dataset consists of 3 hour forecasts from previous cycles serving as a first guess for the next cycle, as opposed to the 6 hour temporal resolution of the Global Reanalysis (GR) (Mesinger et al. 2006). Scaling of the NARR consists of a 32-km grid and 45-layer

resolution (Mesinger et al. 2006). Overlap of some dataset between the first GR and the NARR include rawinsondes, dropsondes, pibals, aircraft, surface, and geostationary satellites. Additional datasets included in the NARR or improved upon from the GR are hourly precipitation, radiances, NCEP surface, MDL surface, Comprehensive Ocean-Atmosphere Dataset (COADS), snow depth, sea surface temperature, sea and lake ice, and tropical cyclones (Mesinger et al. 2006). Of the most interest in regards to this paper, is the observed precipitation assimilation. With this parameter, the model precipitation is more accurate towards the observed precipitation due to the successful assimilation and conversion into latent heat (Mesinger et al. 2006). As opposed to the model forecasting the precipitation, this method is more precise in making a realistic outcome. Hourly precipitation analyses are disaggregated from the NARR using 24 hour rain gauge data (Mesinger et al. 2006). Running tests to compare the reliability of the NARR to actual observed data indicate strong agreement for both winter and summer months (Mesinger et al. 2006).

## 3.2 Methods

### 3.2.1 Case Selection

For this study of precipitation efficiency, three types of cyclone intensities are of interest: explosive, typical, and non-deepening. The classification of cyclone intensities are categorized based on how much or how little pressure drops in the center of the cyclone. For example, the deepening rate of a cyclone is accepted as the largest change in pressure at any given time within the lifecycle of the cyclone. Sanders and Gyakum (1980) talk about classifying an extratropical cyclone as explosive if it has a deepening rate of 1 mb per hour for a 24 hour time period at a latitude of $45^{o}$N. This rate is dependent upon the latitude of the cyclone. The

equation **$24(\sin\Phi/\sin 60^{o})$,** where Φ is the latitude in degrees, is used to calculate the critical rate of a cyclone: 24 mb/24 hr = 1 bergeron (Sanders and Gyakum 1980). This output is used as a threshold to determine whether a cyclone can be classified as explosive dependent upon its latitude. In general, the deepening rate thresholds are higher near the poles and lower towards the equator. Tables 3.1, 3.2, and 3.3 display the lowest central pressure (LCP) obtained throughout the lifecycle of each cyclone, the largest deepening rate within the cyclone's lifecycle obtained within 24 hours, the latitude at which the LCP occurred, and the calculated deepening rate threshold (CDRT). For this study and based on these values, cyclones were determined to be explosive if they were within 3 units of their CDRT. Cyclones are considered typical if deepening rate is between 10 and 4 units from CDRT. For non-deepening cyclones, the deepening rate must be 10 units from CDRT or greater.

Only cyclones that occurred in the cold season months (October through March) were used for this research. Focusing on the cold season minimizes the amount of convective storms analyzed. Research of the warm season and convection has been studied in previous works (eg., Bradbury 1957; Market et al. 2003; Anip and Market 2006). Only cyclones with the majority of their lifecycle in the CONUS were chosen for this study.

Cyclones between the years of 2010 through 2012 were chosen as candidates based on a general search through the Weather Prediction Center's (WPC) surface analysis archive of the US CONUS. To minimize paging through every 3 hour surface analysis, the WPC significant weather event reviews page was used as a general idea for significant cyclone events. NARR data was downloaded in 3 hour increments, from the National Oceanic and Atmospheric Association's (NOAA) National Centers for Environmental Information website, from the development to the decay of each cyclone. To be compatible with our scripts, the .grb files were

Table 3.1 Explosive cases and their lowest central pressure (LCP) in millibars, maximum pressure deepening rate in a 24-hr period, the degree of latitude at which the LCP was achieved, and the calculated deepening rate threshold (CDRT) in millibars.

| Explosive | LCP (mb) | Deepening Rate (mb) | Latitude of LCP (°) | CDRT (mb) |
|---|---|---|---|---|
| 2010 October 25 | 960 | 20 | 46.4 | 20.03883932 |
| 2011 February 13 | 971 | 17 | 48.4 | 20.72358858 |
| 2011 November 09 | 986 | 17 | 41.0 | 18.18124114 |

Table 3.2 Typical cases and their lowest central pressure (LCP) in millibars, maximum pressure deepening rate in a 24-hr period, the degree of latitude at which the LCP was achieved, and the calculated deepening rate threshold (CDRT) in millibars.

| Typical | LCP (mb) | Deepening Rate (mb) | Latitude of LCP (°) | CDRT (mb) |
|---|---|---|---|---|
| 2010 March 21 | 988 | 11 | 43.1 | 18.93543826 |
| 2011 February 17 | 981 | 11 | 50.0 | 21.22924634 |
| 2012 February 28 | 989 | 10 | 41.4 | 18.32681201 |

Table 3.3 Non-deepening cases and their lowest central pressure (LCP) in millibars, maximum pressure deepening rate in a 24-hr period, the degree of latitude at which the LCP was achieved, and the calculated deepening rate threshold (CDRT) in millibars.

| Non-deepening | LCP (mb) | Deepening Rate (mb) | Latitude of LCP (°) | CDRT (mb) |
|---|---|---|---|---|
| 2011 January 28 | 999 | 1 | 44.6 | 19.4586362 |
| 2011 November 05 | 987 | 4 | 49.3 | 21.01003503 |
| 2011 November 26 | 1001 | 6 | 51.7 | 21.74836074 |

converted into GEMPAK files. For the purposes of finding the intensity thresholds and an ideal location to place a grid square for the calculation of PE, the latitude, longitude, and pressure of the cyclone's center is needed for each 3 hour time. Each of these values was manually recorded using IDV.

#### 3.2.1.1 Trial Cases

As a basis for this research, three initial cases are chosen from previous works as examples of explosive, typical, and non-deepening cyclones.

A case study done by Mass and Schultz (1992) over an intense cyclone in the eastern US during 14 – 16 December 1987 provides an example used for an explosive cyclone. This event features a cyclone with various characteristics, such as a strongly deepening pressure center, well defined fronts, and a lifecycle strictly over land on the eastern half of the US (Mass and Schultz 1992). Because of the area this event takes place, data facilities and observation sites are of easy access for the forecasting and recording of this cyclone (Mass and Schultz 1992).Within a 12 hour span of time, between 0000 UTC 15 December 1987 and 1200 UTC 15 December 1987, the central pressure of the cyclone had dropped approximately 23 mb (Mass and Schultz 1992). This more than meets the criteria from Sanders and Gyakum's (1980) paper with a threshold of 20 mb per 24 hour for an explosive cyclone. To produce such an explosively developing cyclone, the main synoptic features associated with it consist of the interactions of long and short wave troughs at both the upper and lower levels of the atmosphere (Mass and Schultz 1992). For more information on the complete synoptic overview of this event, refer to the Mass and Schultz (1992) paper.

A study by Market and Moore (1998) over an extratropical cyclone from 1 – 2 November 1992 represents the example for a typical cyclone case. This cyclone developed over the central US with a lifecycle northward towards the Great Lakes (Market and Moore 1998). Much like the previously mentioned explosive case, the path of this cyclone is land based, allowing for a vast amount of easily obtainable data. As categorized by Market and Moore (1998), this typical cyclone on average produced a deepening rate of -0.5 mb per hour. Based on the criteria for this

research that would fall under a maximum deepening rate per 24 hours of approximately 12 mb. Depending of the latitude of interest, this would most likely be in a typical classification per CDRT. The structure of this cyclone consisted of a typical Norwegian Cyclone Model scheme, specifically due to the layout of frontal features and its lifecycle progressions (Market and Moore 1998). A greater understanding of the synoptic features of the cyclone case can be found in the paper by Market and Moore (1998).

As representation of a non-deepening cyclone, a study by Iskenderian (1987) is done about a cyclone from 03 – 05 March 1985. Similarly to the two previously mentioned cyclones, the Iskenderian (1987) cyclone originates over Colorado and tracks northeastward to the furthest northeastern states of the US. In this non-developing cyclone, the first 12 hours, from 1200 UTC 04 March 1985 to 0000 UTC 05 March 1985, consist of little to no change in central pressure (Iskenderian 1987). Interestingly in the next 12 hours, the cyclone's central pressure actually increases by 14 mb from 0000 UTC 05 March 1985 to 1200 UTC 05 March 1985 (Iskenderian 1987). This cyclone is well within the requirements to be considered non-deepening. Further information on the structure of this cyclone can be found from Iskenderian (1987).

#### 3.2.1.2 WPC archived cases

To establish a workable case size, three cyclones representing each intensity classification are chosen, in addition to the three original trial cases. Tables 3.4.a,b, and c show the change in the lowest central pressure as each explosive cyclone develops, and the latitude and longitude at which the center of the cyclone progresses, all at the three hour intervals of the NARR data. Tables 3.5.a, b, and c and Tables 3.6.a, b, and c show the same date except for typical and non-deepening cases, respectively. In reference to the eulerian method, Tables 3.7,

3.8, and 3.9 show the explosive, typical, and non-deepening cyclones, respectively, of the time, latitude, longitude, and central pressure of the grid square placed in the path of each moving cyclone in order to calculate the precipitation efficiency.

The first explosive cyclone chosen for this research takes place on 0900 UTC 25 October 2010 through 1800 UTC 28 October 2010. This system originates over northern Colorado and tracks north/northeastward to Ontario. Secondly, the explosive cyclone from 0000 UTC 13 February 2011 to 1200 UTC 16 February 2011 originates over the Oklahoma/Arkansas border and decays northeast of Maine. Lastly, the explosive cyclone from 0300 UTC 09 November 2011 to 0900 UTC 11 November 2011 begins over Missouri and tracks towards Ontario. Because the lifecycle of these cyclones stretch over a few days' time, an Eulerian approach of calculating the precipitation efficiency was also taken where a box is placed in the path of each cyclone. This method is discussed in greater detail in the next section. Figures 3.1.a, b, and c, display the location of each explosive cyclone's central pressure at the times chosen for the grid square PE calculation for the eulerian method.

With the classification of typical cyclones, the first cyclone develops on 2100 UTC 21 March 2010 and continues through 1200 UTC 25 March 2010. This cyclone develops over Arkansas, moving northeast and decays over Maine. Also classified as typical, the cyclone from 1200 UTC 17 February 2011 through 0900 UTC 19 February 2011 develops over the North and South Dakota border and travels with a generally easterly direction and decays over Maine. The final typical cyclone is from 1500 UTC 28 February 2012 through 2100 UTC 01 March 2012 and forms over Colorado, traveling northeast toward New York. Figures 3.2.a, b, and c, display the location of each typical cyclone's central pressure at the time chosen to place the grid square in the eulerian method.

Table 3.4.a. Explosive case 25 – 28 October 2010 displaying the time, latitude, longitude, and lowest central pressure in three hour increments from development to decay.

| 2010 October 25 | | | |
|---|---|---|---|
| Time (UTC) | Latitude | Longitude | Pressure (mb) |
| 0900 | 44.1 | -102.4 | 983 |
| 1200 | 43.8 | -101.7 | 982 |
| 1500 | 42.3 | -100.7 | 985 |
| 1800 | 39.1 | -99.9 | 983 |
| 2100 | 40 | -97.6 | 982 |
| 26/000 | 41.6 | -95.7 | 980 |
| 0300 | 43.3 | -95.1 | 979 |
| 0600 | 44.4 | -94.4 | 974 |
| 0900 | 45.3 | -94.7 | 972 |
| 1200 | 46.4 | -94.3 | 971 |
| 1500 | 46.7 | -94.3 | 965 |
| 1800 | 47.4 | -94.1 | 964 |
| 2100 | 48.1 | -93.9 | 961 |
| 27/0000 | 48.2 | -93.4 | 960 |
| 0300 | 48.5 | -93.2 | 960 |
| 0600 | 48.6 | -93.1 | 962 |
| 0900 | 49.2 | -92 | 965 |
| 1200 | 49.7 | -91.5 | 969 |
| 1500 | 50.2 | -89.8 | 970 |
| 1800 | 50.7 | -89.4 | 975 |
| 2100 | 51.2 | -87.8 | 978 |
| 28/0000 | 52.1 | -86.7 | 981 |
| 0300 | 52 | -85.3 | 983 |
| 0600 | 54.5 | -82.4 | 985 |
| 0900 | 54.9 | -83.6 | 986 |
| 1200 | 55.9 | -80.7 | 988 |
| 1500 | 52.8 | -81.6 | 989 |
| 1800 | 56.7 | -80.7 | 991 |

Table 3.4.b. Explosive case 13 – 16 February 2011 displaying the time, latitude, longitude, and lowest central pressure in three hour increments from development to decay.

| 2011 February 13 | | | |
|---|---|---|---|
| Time (UTC) | Latitude | Longitude | Pressure (mb) |
| 0000 | 55.2 | -124.3 | 992 |
| 0300 | 54 | -118 | 987 |
| 0600 | 53 | -114.6 | 984 |
| 0900 | 52.7 | -111.2 | 985 |
| 1200 | 52.2 | -108 | 985 |
| 1500 | 50.7 | -102.6 | 984 |
| 1800 | 49.7 | -99 | 986 |
| 2100 | 48.3 | -94.5 | 988 |
| 14/0000 | 47.9 | -91.8 | 991 |
| 0300 | 46.7 | -87.8 | 988 |
| 0600 | 46.1 | -85.3 | 987 |
| 0900 | 45.4 | -81.4 | 988 |
| 1200 | 45.5 | -77.6 | 989 |
| 1500 | 45.7 | -75.4 | 988 |
| 1800 | 45.7 | -71.3 | 991 |
| 2100 | 44.5 | -68.2 | 991 |
| 15/0000 | 44.8 | -67.2 | 992 |
| 0300 | 45.8 | -63.7 | 992 |
| 0600 | 45.5 | -62 | 991 |
| 0900 | 46.2 | -60.2 | 989 |
| 1200 | 46.3 | -58.9 | 987 |
| 1500 | 47.2 | -56.9 | 986 |
| 1800 | 47.2 | -55.4 | 987 |
| 2100 | 48.4 | -53.4 | 980 |
| 16/0000 | 49.2 | -53.1 | 978 |
| 0300 | 49.8 | -51.7 | 977 |
| 0600 | 50 | -51.7 | 982 |
| 0900 | 50.7 | -47.8 | 971 |
| 1200 | 51.5 | -47.2 | 971 |

Table 3.4.c. Explosive case 09 – 11 November 2011 displaying the time, latitude, longitude, and pressure in three hour increments from development to decay.

| 2011 November 09 | | | |
|---|---|---|---|
| Time (UTC) | Latitude | Longitude | Pressure (mb) |
| 0300 | 37.9 | -93.4 | 1010 |
| 0600 | 38.4 | -91.3 | 1008 |
| 0900 | 39.9 | -90 | 1006 |
| 1200 | 41 | -89.5 | 1004 |
| 1500 | 47.4 | -87.3 | 1004 |
| 1800 | 44 | -86.2 | 999 |
| 2100 | 44.9 | -85.1 | 997 |
| 10/0000 | 46.4 | -84.1 | 995 |
| 0300 | 47.1 | -83.6 | 993 |
| 0600 | 48 | -82.9 | 991 |
| 0900 | 49.1 | -81.8 | 991 |
| 1200 | 50.3 | -81.3 | 989 |
| 1500 | 51.4 | -80.2 | 989 |
| 1800 | 52.5 | -79.9 | 989 |
| 2100 | 53.6 | -79.2 | 989 |
| 11/0000 | 55.2 | -77.8 | 989 |
| 0300 | 55.8 | -77.6 | 986 |
| 0600 | 56.5 | -77.2 | 986 |
| 0900 | 57.2 | -77.3 | 986 |

The non-deepening cyclone from 0600 UTC 28 January 2011 through 1800 UTC 29 January 2011 originates over Alberta and moves southeast and decays over Ohio. The second non-deepening cyclone from 1800 UTC 05 November 2011 through 2100 UTC 07 November 2011 develops over Colorado and decays over Ontario. Lastly, the non-deepening cyclone from 0000 UTC 26 November 2011 through 2100 UTC 28 November 2011 develops over Nebraska and decays northeast Maine. For the eulerian method of calculating PE, Figures 3.3.a, b and c, show the locations of each non-deepening cyclone's central pressure at the time chosen for the grid square.

Table 3.5.a. Typical case 21 – 25 March 2010 displaying the time, latitude, longitude, and lowest central pressure in three hour increments from development to decay.

| 2010 March 21 | | | |
|---|---|---|---|
| Time (UTC) | Latitude | Longitude | Pressure (mb) |
| 2100 | 35.6 | -85.5 | 1005 |
| 22/0000 | 37.2 | -86.9 | 1005 |
| 0300 | 37.7 | -87.8 | 1004 |
| 0600 | 37.6 | -88.4 | 1006 |
| 0900 | 37.5 | -88.9 | 1004 |
| 1200 | 36.8 | -89.7 | 1007 |
| 1500 | 40.3 | -81.1 | 1006 |
| 1800 | 38.5 | -81.4 | 1006 |
| 2100 | 39.3 | -80.7 | 1001 |
| 23/0000 | 40 | -80.8 | 1000 |
| 0300 | 40 | -80.8 | 1000 |
| 0600 | 40.7 | -79.7 | 1001 |
| 0900 | 39.9 | -77.1 | 1001 |
| 1200 | 40.9 | -77.7 | 1000 |
| 1500 | 41.5 | -75.5 | 1001 |
| 1800 | 42.2 | -74.7 | 999 |
| 2100 | 42.1 | -69.7 | 996 |
| 24/0000 | 42.5 | -69.4 | 994 |
| 0300 | 43.1 | -69 | 992 |
| 0600 | 43 | -69.2 | 991 |
| 0900 | 42.5 | -68.2 | 991 |
| 1200 | 42.5 | -66.3 | 992 |
| 1500 | 45.2 | -63.7 | 990 |
| 1800 | 45.5 | -62.8 | 989 |
| 2100 | 46.4 | -62.2 | 990 |
| 25/0000 | 47 | -61.7 | 988 |
| 0300 | 47.9 | -61.4 | 988 |
| 0600 | 48.4 | -60.8 | 988 |
| 0900 | 48.6 | -60.4 | 989 |
| 1200 | 47.1 | -55.8 | 991 |

Table 3.5.b. Typical case 17 – 19 February 2011 displaying the time, latitude, longitude, and lowest central pressure in three hour increments from development to decay.

| 2011 February 17 | | | |
|---|---|---|---|
| Time (UTC) | Latitude | Longitude | Pressure (mb) |
| 1200 | 44.7 | -101.6 | 991 |
| 1500 | 45.1 | -96.4 | 993 |
| 1800 | 47.9 | -91.5 | 990 |
| 2100 | 48.2 | -91.6 | 991 |
| 18/0000 | 50.4 | -92.8 | 992 |
| 0300 | 50 | -91 | 988 |
| 0600 | 49.5 | -87.6 | 988 |
| 0900 | 50.6 | -87.8 | 986 |
| 1200 | 50.7 | -83.3 | 984 |
| 1500 | 51.4 | -81.5 | 982 |
| 1800 | 51.9 | -79.8 | 981 |
| 2100 | 52.4 | -78.6 | 982 |
| 19/0000 | 53 | -77.8 | 981 |
| 0300 | 53.2 | -77.1 | 985 |
| 0600 | 53.6 | -76.4 | 987 |
| 0900 | 49.3 | -67.6 | 992 |

Table 3.5.c. Typical case 28 February 2012 through 01 March 2012 displaying the time, latitude, longitude, and pressure in three hour increments from development to decay.

| 2012 February 28 | | | |
|---|---|---|---|
| Time (UTC) | Latitude | Longitde | Pressure (mb) |
| 1500 | 41.4 | -105.4 | 999 |
| 1800 | 40.2 | -102.4 | 997 |
| 2100 | 40.8 | -101.7 | 996 |
| 29/0000 | 41.2 | -99.7 | 995 |
| 0300 | 41.4 | -98.1 | 995 |
| 0600 | 41.6 | -96 | 992 |
| 0900 | 42.7 | -94.3 | 994 |
| 1200 | 43.5 | -93.4 | 991 |
| 1500 | 44.3 | -92.8 | 989 |
| 1800 | 44.3 | -92.8 | 990 |
| 2100 | 44.7 | -90.3 | 995 |
| 03/01/0000 | 44.3 | -90.3 | 998 |
| 0300 | 45.1 | -87.7 | 998 |
| 0600 | 42.8 | -80.6 | 1001 |
| 0900 | 42.9 | -78 | 999 |
| 1200 | 43.5 | -77.2 | 1002 |
| 1500 | 42.1 | -75.5 | 1004 |
| 1800 | 39.9 | -61.8 | 1000 |
| 2100 | 39.8 | -59.3 | 1002 |

Table 3.6.a. Non-deepening case 28 – 29 January 2011 displaying the time, latitude, longitude, and lowest central pressure in three hour increments from development to decay.

| 2011 January 28 | | | |
|---|---|---|---|
| Time (UTC) | Latitude | Longitude | Pressure (mb) |
| 0600 | 55 | -107.4 | 999 |
| 0900 | 54.3 | -105.7 | 999 |
| 1200 | 52.6 | -102.6 | 1000 |
| 1500 | 52 | -101 | 1001 |
| 1800 | 48.9 | -98.6 | 1001 |
| 2100 | 48.2 | -96 | 1002 |
| 29/0000 | 48 | -85.3 | 1005 |
| 0300 | 45.5 | -92.1 | 1006 |
| 0600 | 44.6 | -90.7 | 1005 |
| 0900 | 43.9 | -87.6 | 1005 |
| 1200 | 43.2 | -86.8 | 1005 |
| 1500 | 43 | -86.1 | 1005 |
| 1800 | 41.7 | -82.2 | 1010 |

Table 3.6.b. Non-deepening case 05 – 07 November 2011 displaying the time, latitude, longitude, and lowest central pressure in three hour increments from development to decay.

| 2011 November 05 | | | |
|---|---|---|---|
| Time (UTC) | Latitude | Longitude | Pressure (mb) |
| 1800 | 44.1 | -103.6 | 988 |
| 2100 | 43.8 | -103.2 | 987 |
| 06/0000 | 42.2 | -102 | 992 |
| 0300 | 43.8 | -100.5 | 993 |
| 0600 | 48 | -99.2 | 994 |
| 0900 | 48.7 | -98.8 | 992 |
| 1200 | 49.3 | -98.6 | 992 |
| 1500 | 49.8 | -98.1 | 990 |
| 1800 | 50.5 | -97.6 | 989 |
| 2100 | 51.3 | -97 | 990 |
| 07/0000 | 52 | -96.1 | 990 |
| 0300 | 52.2 | -95.7 | 992 |
| 0600 | 52.7 | -94.6 | 994 |
| 0900 | 54.3 | -89.9 | 996 |
| 1200 | 55.1 | -88.1 | 996 |
| 1500 | 55.6 | -82.1 | 993 |
| 1800 | 56.1 | -81.2 | 995 |
| 2100 | 56.5 | -78.7 | 996 |

Table 3.6.c. Non-deepening case 26 – 28 November 2011 displaying the time, latitude, longitude, and pressure in three hour increments from development to decay.

| 2011 November 26 | | | |
|---|---|---|---|
| Time (UTC) | Latitude | Longitude | Pressure (mb) |
| 0000 | 41 | -99.8 | 1004 |
| 0300 | 44.1 | -96.2 | 1003 |
| 0600 | 36.1 | -98.6 | 1006 |
| 0900 | 39.1 | -96.3 | 1006 |
| 1200 | 44.9 | -92 | 1006 |
| 1500 | 45.6 | -91 | 1006 |
| 1800 | 46 | -88.9 | 1006 |
| 2100 | 47.1 | -86.9 | 1007 |
| 27/0000 | 47.2 | -86.1 | 1007 |
| 0300 | 47.7 | -85.8 | 1008 |
| 0600 | 47.7 | -84.3 | 1008 |
| 0900 | 48 | -82.6 | 1008 |
| 1200 | 47.6 | -81.7 | 1008 |
| 1500 | 49.3 | -80.4 | 1006 |
| 1800 | 49.4 | -78.4 | 1004 |
| 2100 | 49.6 | -76.8 | 1005 |
| 28/0000 | 50.8 | -76.3 | 1004 |
| 0300 | 51.1 | -74.7 | 1006 |
| 0600 | 51.5 | -73.9 | 1005 |
| 0900 | 51.8 | -71.9 | 1005 |
| 1200 | 51.7 | -69.2 | 1007 |
| 1500 | 51.7 | -64.7 | 1002 |
| 1800 | 50.3 | -61.1 | 1001 |
| 2100 | 50.7 | -58.6 | 1001 |

Table 3.7 Explosive cases used in the eulerian method. The time is chosen as a focal point in which the grid box is placed for the calculation of PE. The cyclone's central pressure is recorded at the time chosen and the degrees of latitude and longitude are the location of the cyclone's central pressure at that time.

| Explosive | Time (UTC) | Central Pressure (mb) | Latitude (deg) | Longitude (deg) |
|---|---|---|---|---|
| 2010 October 25 | October 26, 2100 | 961 | 48.1 | -93.9 |
| 2011 February 13 | February 14, 0600 | 987 | 46.1 | -85.3 |
| 2011 November 09 | November 09, 2100 | 997 | 44.9 | -85.1 |

Table 3.8. Typical cases used in the eulerian method. The time is chosen as a focal point in which the grid box is placed for the calculation of PE. The cyclone's central pressure is recorded at the time chosen and the degrees of latitude and longitude are the location of the cyclone's central pressure at that time.

| Typical | Time (UTC) | Central Pressure (mb) | Latitude (deg) | Longitude (deg) |
|---|---|---|---|---|
| 2010 March 21 | March 23, 2100 | 996 | 42.1 | -69.7 |
| 2011 February 17 | February 18, 0000 | 992 | 50.4 | -92.8 |
| 2012 February 28 | February 29, 1200 | 991 | 43.5 | -93.4 |

Table 3.9. Non-deepening cases used in the eulerian method. The time is chosen as a focal point in which the grid box is placed for the calculation of PE. The cyclone's central pressure is recorded at the time chosen and the degrees of latitude and longitude are the location of the cyclone's central pressure at that time.

| Non-deepening | Time (UTC) | Central Pressure (mb) | Latitude (deg) | Longitude (deg) |
|---|---|---|---|---|
| 2011 January 28 | January 28, 2100 | 1002 | 48.2 | -96.0 |
| 2011 November 05 | November 06, 0900 | 992 | 48.7 | -98.8 |
| 2011 November 26 | November 27, 0000 | 1007 | 47.2 | -86.1 |

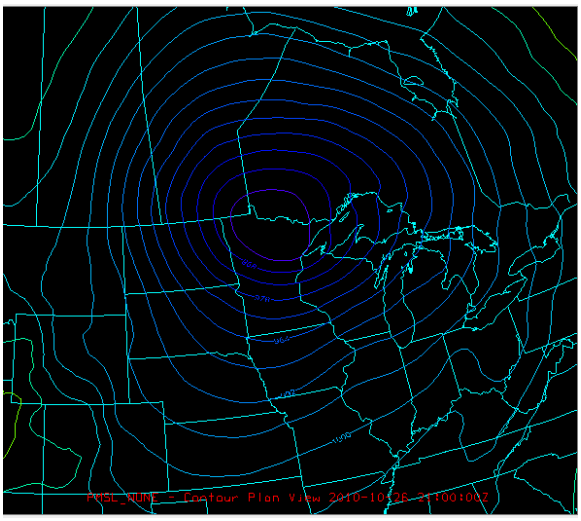

Fig. 3.1.a. Analysis of sea level pressure (solid; every 4 mb) for an explosive case valid at 2100 UTC 26 October 2010.

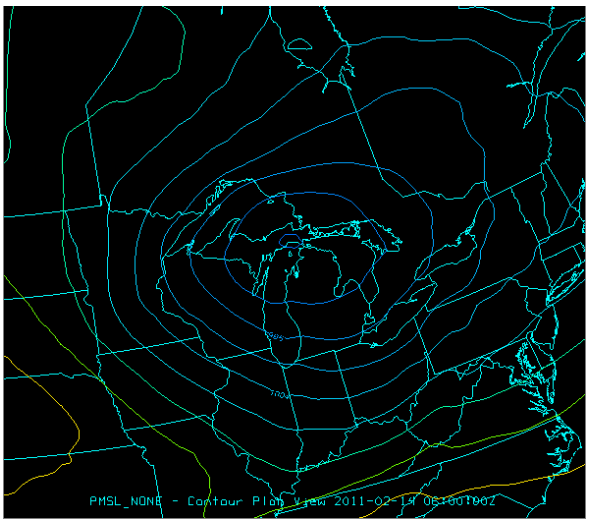

Fig. 3.1.b. Analysis of sea level pressure (solid; every 4 mb) for an explosive case valid at 0600 UTC 14 February 2011.

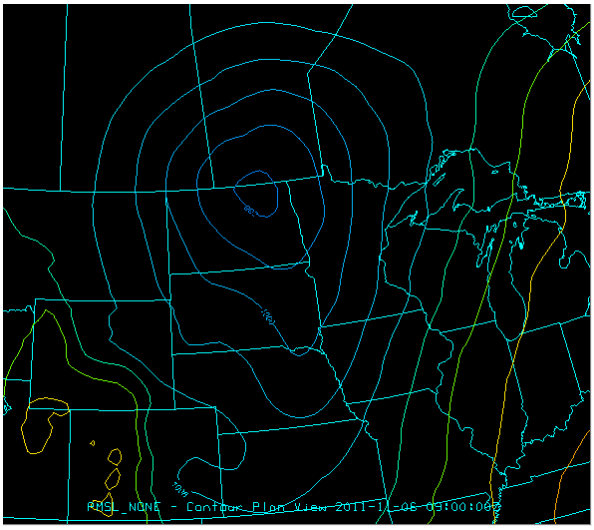

Fig. 3.1.c. Analysis of sea level pressure (solid; every 4 mb) for an explosive case valid at 2100 UTC 09 November 2011.

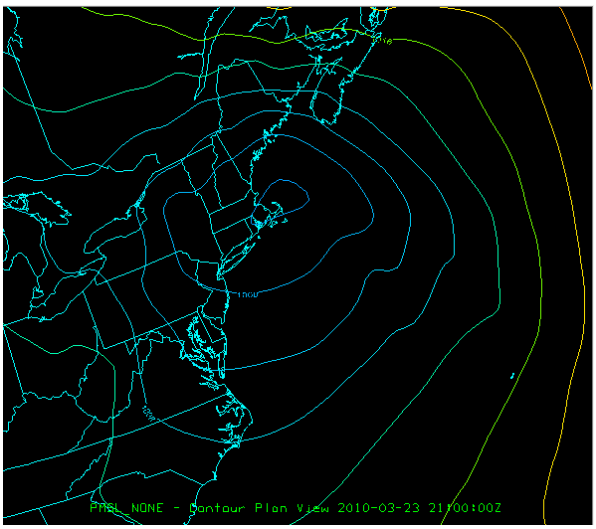


Fig. 3.2.a. Analysis of sea level pressure (solid; every 4 mb) for a typical case valid at 2100 UTC 23 March 2010.

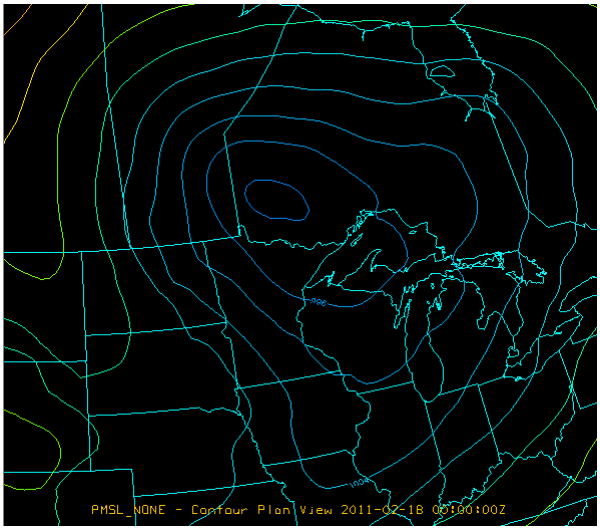


Fig. 3.2.b. Analysis of sea level pressure (solid; every 4 mb) for a typical case valid at 0000 UTC 18 February 2011.

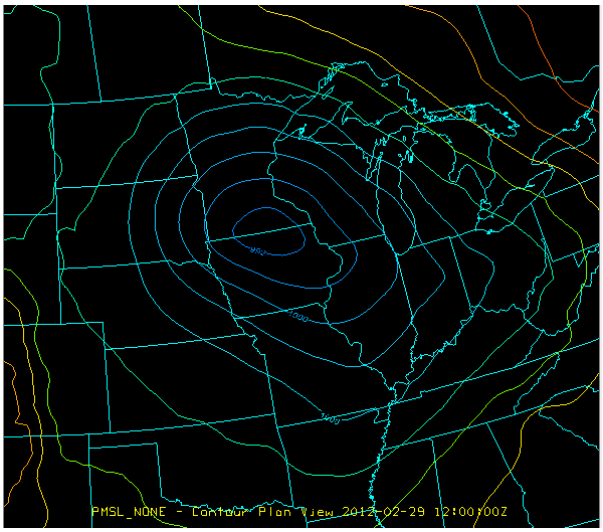


Fig. 3.2.c. Analysis of sea level pressure (solid; every 4 mb) for a typical case valid at 1200 UTC 29 February 2012.

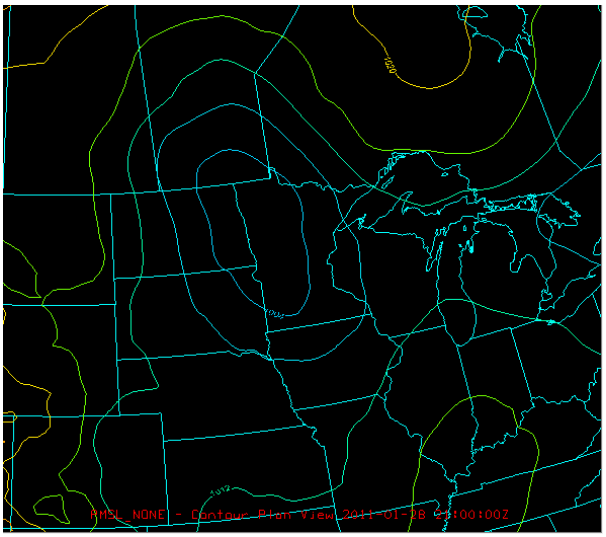

Fig. 3.3.a. Analysis of sea level pressure (solid; every 4 mb) for a non-deepening case valid at 2100 UTC 28 January 2011.

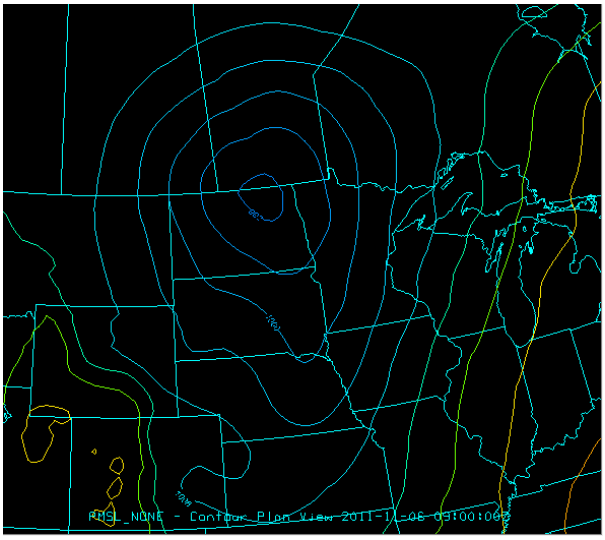

Fig. 3.3.b. Analysis of sea level pressure (solid; every 4 mb) for a non-deepening case valid at 0900 UTC 06 November 2011.

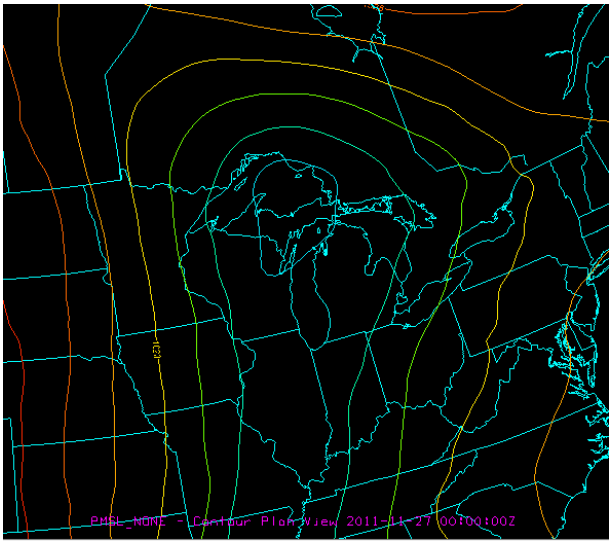

Fig. 3.3.c. Analysis of sea level pressure (solid; every 4 mb) for a non-deepening case valid at 0000 UTC 27 November 2011.

### 3.2.2 PE calculation method

The expression employed here derives from Doswell et al. (1996) and their appendix:

$$m_p = \int_T \left( \iint_A \rho_w R dx dy \right) dt \tag{1}$$

and moisture ingested

$$m_i = \int_T \left[ \iiint_\Sigma \nabla \bullet \left( \rho q \vec{V} \right) dx dy dz \right] dt \tag{2}$$

where in (1) $T$ is the life time of the MCS, $A$ is the area of integration, $\rho_w$ is the density of water, and R is the rainfall rate, and in (2), $\Sigma$ is the volume of integration, $\rho$ is the air density, $q$ is the mixing ratio, and $\boldsymbol{V}$ is the three-dimensional wind velocity. This is the most robust approach, and effectively envelops a precipitating system in an envelope through which ingested moisture must pass, both horizontally and vertically. Doswell et al. (1996) focused primarily on convection; here we adopt the approach to transient extratropical cyclones. Although more time consuming, we employ this approach also because there is no other method that is comparable for calculating or estimating PE for individual precipitating systems (Pettegrew 2004). The PE calculations were performed in GEMPAK using a series of scripts. The first script (*PE0.csh*) interpolates values in the NARR grids to every 50 mb for levels above 500 mb. The second script (*PE1.csh*) calculates the moisture flux divergence at every pressure in the entire NARR grid domain up to 300 mb and then integrates it in geometric (*z*) space for each grid element volume (*dx* X *dy* X *dz*). The third script (*PE2.csh*) masks out all non-atmospheric grid levels that were actually below the real model surface, and for which no real data were truly observed (Fig. 3.4). The fourth script (*PE3.csh*) sums up each column with real integrated moisture flux divergence values through 300 mb. The final (*PE4.*csh) script converts the 3-hour accumulated precipitation to a mass, and

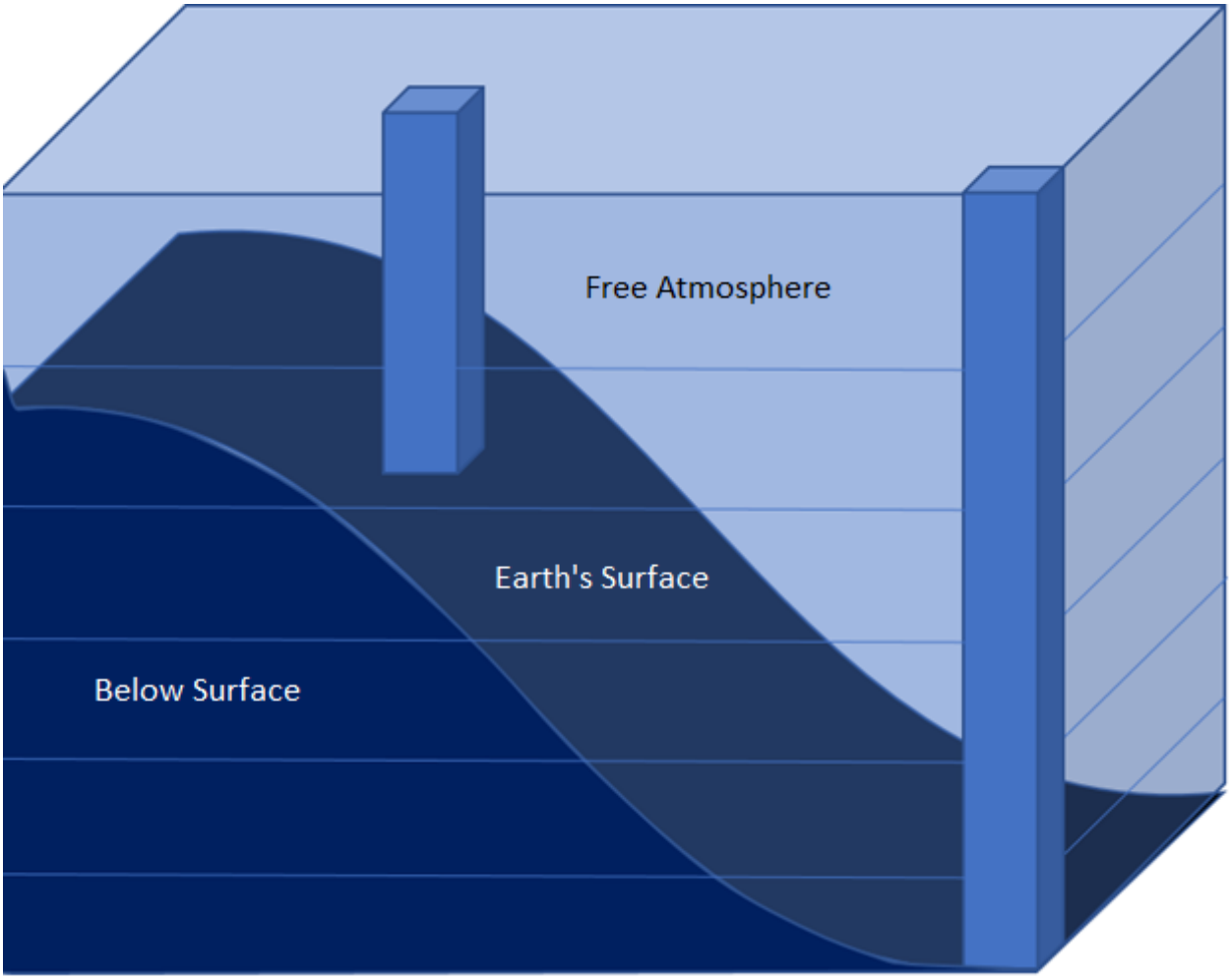


Fig. 3.4. A schematic example of masking the difference in columns used for moisture flux divergence calculations.

masks out any grid elements where precipitation did not fall. Each cyclone at every 3-hour time interval was processed through these scripts. For both the lagrangian and eulerian method, a grid space of 5 degrees latitude and 10 degrees longitude is used for the calculation of PE. In the mid-latitudes, this is roughly 600 X 600 km.

# Chapter 4. Analysis

## 4.1 Trial Cases

The three trial cases in this research represent our control group for experimenting with multiple other cyclone cases of different intensities and how to calculate their PE. After calculations, the explosive case, 14 December 1987, resulted in a total storm precipitation efficiency of 22%. The typical case, 01 November 1992, resulted in a total storm PE of 11%. Lastly, the non-deepening case, 03 March 1985, had an average storm total PE of -4%. As expected, the explosive case presents the highest value of PE, the typical case, second highest, and the non-deepening case represents the lowest PE. Though these cyclonic events are nowhere near 100%, or even 50% efficient, multiple reasons have been discussed on *loss* of water mass in Chapter 2. Of all the cases shown, these were selected first and subjected to very careful screening and calculation, prior to going forward in "production mode." As such, they are likely the most reliable.

## 4.2 Additional Cases

### 4.2.1 Lagrangian Method

Using an additional sample of nine cases, three explosive, three typical, and three non-deepening cyclones, experiments were done using the lagrangian method of calculating PE. For this method, PE was calculated for each 3 hour time interval at the latitude and longitude of the lowest central pressure relevant to that time. In essence, there is a moving box around the center of each cyclone that calculates the PE of the cyclone as it grows and decays across North America. Similar to the PE calculation method of the trial cases, the average PE of the entire storm is converted into the storm total PE. The three explosive cases result in PEs of 20%, -21%,

and -9%. The three typical cases have calculated PEs of 8%, 556%, and -20%. Lastly, the non-deepening cyclones resulted in PEs of -15%, -27%, and 34%. Compared to the trial cases, the explosive cyclone PE results are similar in scale, aside from two of the values being negative. The typical case of 21 March 2010 presents a similar PE to that of the trial case at 8%. The case of 17 February 2011 results in an outrageously large PE. If the instantaneous PE at time 0600 UTC 18 February 2011 of 9870% is negated from the storm total PE, the outcome is a -32%. The non-deepening case PEs, were expected to be smaller than what was obtained. The case 2011 November 26 was the only cyclone that resulted in a positive PE value. A PE of 34% for a non-deepening cyclone seems extravagant.

Speculations as to why the PE resulted in so many large values could be due to errant (or missing) values in the NARR native grids and cyclones approaching the grid's edge. Errors could also be due to the PE being calculated over the entire life cycle of the cyclone, each of which may last from 36 hours to 84 hours and beyond. In an attempt to mitigate this issue, a 24-hour window, in which the lowest central pressure of the cyclone is centered, is used to calculate PE. These results can be found in Table 4.1. This approach was designed to normalize the method of calculating PE across all ETCs. Cases in which negative values were of result did not change significantly in a positive direction. The typical case 21 March 2010 that initially resulted in a similar PE to the trial cases of 8%, resulted in a PE of 118%. The typical case, 17 February 2011, that originally resulted in a very large PE of 556% now resulted in a PE of 993%. In contrast with these typical case PEs blowing up, the non-deepening cyclone, 26 November 2011, changed from a PE of 34% to 3%. For a non-deepening cyclone this is a much closer value that is expected. The non-deepening cyclone, 05 November 2011, also changes from a PE of -27% to a -8%. Although the value is still negative, it is a step closer to 0% at least.

### 4.2.2 Eulerian Method

Because the PE values achieved from the lagrangian method require a great deal of manual intervention, a different approach was done in an attempt to achieve a more automated result. Instead of calculating the PE at each 3-hour time interval centered at the corresponding latitude and longitude of the cyclone center, an eulerian method was established where one grid is placed at a particular time, latitude, and longitude, and PE is calculated as the cyclone progresses through this box. Also, instead of calculating the PE for each 3 hour time interval and then averaging them, the moisture flux divergence (*mi*) and accumulated 3 hour precipitation (*mp*) are calculated for each time interval and then summed and averaged at the final calculation. With this method, the explosive cyclones resulted in PE values of -59012%, -1208%, and 70%. Resulting PE calculations for the typical cyclones are 227%, 169%, and 86%. For the three non-deepening cyclones, PE results are 377%, 98%, and 1202%. This eulerian method produces extremely large values of PE for all three cyclone intensities. Interestingly, only two explosive cases have negative values, whereas every other case, explosive, typical, and non-deepening, are positive values of PE. These extreme values could be due to the focus on only one area letting the cyclone progress through, or even too small of a calculation area.

## 4.3 Summary

After calculating the precipitation efficiency of multiple different extratropical cyclones of various intensities, many differences have been found from the methods of calculating their PE. The three trial cases, one of each explosive, typical, and non-deepening cyclones, resulted in acceptable PE values with the lagrangian method. As expected, the explosively developing cyclone produced the highest PE, and the non-developer with the lowest PE. Using the eulerian

Table 4.1. PE results for each cyclone case for the lagrangian and eulerian methods.

| Intensity | Date | PE Lagrangian Lifetime | PE Lagrangian 24-hr | PE Eulerian |
|---|---|---|---|---|
| Explosive | 1987 December 14 | 22% | 32% | -35% |
| | 2010 October 25 | 20% | 70% | -59012% |
| | 2011 February 13 | -21% | -29% | -1208% |
| | 2011 November 09 | -9% | -23% | 70% |
| | **PE Average** | 3% | 13% | -15046% |
| | **PE Std Dev** | 21% | 47% | 29316% |
| Typical | 1992 November 01 | 11% | 11% | -12% |
| | 2010 March 21 | 8% | 118% | 252% |
| | 2011 February 17 | 556% | 993% | 170% |
| | 2012 February 28 | -20% | -19% | 87% |
| | **PE Average** | 138% | 275% | 124% |
| | **PE Std Dev** | 278% | 481% | 113% |
| Non-developers | 1985 March 03 | -4% | -6% | -5% |
| | 2011 January 28 | -15% | -21% | 377% |
| | 2011 November 05 | -27% | -8% | 98% |
| | 2011 November 26 | 34% | 3% | 1202% |
| | **PE Average** | 3% | -8% | 418% |
| | **PE Std Dev** | 26% | 10% | 547% |

method, each of the trial cases resulted in a negative value of PE. The lagrangian method for calculating PE used on the 9 additional cases resulted in various values of PE, with one extremely large PE. In an attempt to attain similar values to the initial trial case runs, a 24-hour window was used to calculate PE that resulted in still somewhat contrary values. After calculating the PE of the additional 9 cases using the eulerian method, it was concluded this is

not the favorable approach. Extremely large values of PE were calculated for many of the cyclone cases. Multiple variables could be of consequence in the unacceptable values of PE. A smaller grid box was used to calculate PE for the 9 additional cases, thus narrowing the window in which precipitation is ingested. In some cases, the PE is thrown out of proportion by individually large or small instantaneous values.

In the end, it is clear that the current methods are not acceptable for the intended purpose, and not yet ready for broader use. The individual values for PE, as well as their average and standard deviation in Table 4.1, demand 1) a return to software development and/or 2) much more extensive testing on a far greater sample of cases events.

## Chapter 5. Conclusions

Forecasting rainfall has been a staple of meteorological research for over a century. Questions of when will it rain, where will it rain, how much will it rain, and how long will it rain are never ending challenges for forecasters. A step forward in answering these questions comes into play with the study of precipitation efficiency. PE is defined as the ratio between water vapor into a cyclone and the precipitated water. Different methods for calculating PE have been documented in recent history, specifically the Doswell et al. (1996) suggestion of a lagrangian method, where the PE is calculated as the cyclone is moving. Pettegrew (2004) also evaluated and rejected most methods of PE estimation other than the full equation method. The main objective of this research was to use experimental software to determine a suitable method of calculating PE. Several different cyclones were examined, ranging in intensities from explosive, to typical, and non-deepening, and analyzed to find which classification supported the highest PE.

The NARR dataset was used as the primary resource for attaining 3-hour accumulated precipitation for the lifespan of each cyclone. Each cyclone classification was determined based on a threshold of the deepening of central pressure calculated based on the latitude of each cyclone. Explosive cyclones exhibited the greatest pressure deepening rates, whereas a non-deepening cyclone portrayed the smallest pressure drops.

The three trial cases were well documented cyclones. A lagrangian method of calculating PE resulted in a strong sample for the trial cases. The explosive case represented the cyclone with the largest PE, and the non-deepening cyclone with the lowest PE as was hypothesized. Additional cases were chosen to broaden the sample size and experiment with different methods of calculating PE.

The additional 9 cases, using the lagragian method and average PE for the entirety of the cyclones lifecycle, displayed a wide array of PE results both negative and positive. Another lagrangian approach was done using a 24-hour time centered around the lowest central pressure of each cyclone. Negative and positive values of PE were still obtained with a couple cases resulting in extravagantly large values of PE. An eulerian method was then used to calculate PE and resulted very large values of PE for all of the additional 9 cases. For the trial cases with this method, each value calculated as a negative PE.

The three trial cases are probably the most accurate, given the time invested in their preparation. Unfortunately, the sample size is too small to say this with confidence. The most realistic method for calculating PE appears to be the pure lagrangian approach. However, even with a total sample size of only 12, the erratic behavior in the PE values shows that more work needs to be done on the method and/or code for PE calculation.

It is clear that further work and experimentation will be necessary before consistently acceptable estimates of cyclone PE can be calculated.

## References


Anip, M. H. and P. Market, 2006: Dominant factors influencing precipitation efficiency in a continental mid-latitude location. *Tellus*, 1-5.

Bradbury, D. L. 1957: Moisture analysis and water budget in three different types of storms. *J. Meteor*., **14**, 559-565.

Doswell, C. A., H. E. Brooks, and R. A. Maddox, 1996: Flash flood forecasting: an ingredients-based- methodology. *Wea. Forecasting*, **11**, 560-581.

Iskenderian, H., 1987: Three-dimensional airflow and precipitation structure in a non-deepening cyclone. *Mon. Wea. Rev.*, **3**, 18-32.

Market, P.S., S. Allen, R. Scofield, R. Kuligowski and A. Gruber, 2003: Precipitation efficiency of warm-season Midwestern mesoscale convective systems. *Wea. Forecast.* **18**, 1273-1285.

Market, P. S. and J. T. Moore, 1997: Mesoscale evolution of a continental occluded cyclone. *Mon. Wea. Rev.*, **126**, 1793-1811.

Mass, C. F. and D. M. Schultz, 1992: The structure and evolution of a simulated midlatitude cyclone over land. *Mon. Wea. Rev.*, **121**, 889-917.

Mesinger, F., G. DiMego, E. Kalnay, K. Mitchell, P. C. Shafran, W. Ebisuzaki, D. Jovic, J. Woollen, E. Rogers, E. H. Berbery, M. B. Ek, Y. Fan, R. Grumbine, W. Higgins, H. Li, Y. Lin, G. Manikin, D. Parrish, and W. Shi, 2006: North American Regional Reanalysis. *Bull. Of Amer. Meteor. Soc.*, **87**, 343-359.

Pettegrew, B., 2004: On methods of precipitation efficiency estimation.

Rasmussen, J.L., R. W. Furman, and H. Riehl, 1969: Moisture analysis of an extratropical cyclone. *Arch. Met. Geoph. Biokl*, **18**, 275-298.

Robinson, P. J., and J. T. Lutz, 1978: Precipitation efficiency of cyclone storms. *Assoc. of Amer.*

*Geographers*, **68**-1, 81-88.

Rockel, B., and U. Karstens, 2001: Development of the water budget for three extra-tropical cyclones with intense rainfall over Europe. *Meteor. and Atmos. Physics*, **77**, 75-83.

Sanders, F. and J. R. Gyakum, 1980: Synoptic-dynamic climatology of the "Bomb". *Mon. Wea. Rev.*, **108**, 1589-1606.

Sellers, W. D., 1965: Physical Climatology. *University of Chicago*, 4-10.

Sui, C. H., X. Li, M. Yang, 2007: On the definition of precipitation efficiency. *Journal of Atmo. Sciences*, **64**, 4506-4513.

# Appendix A

```
:::::::
PE0.csh
:::::::

#!/bin/sh

# Get standard settings
LD_LIBRARY_PATH=/opt/SUNWspro/lib:/usr/X11R6/lib:/usr/lib
export LD_LIBRARY_PATH

rm gemglb.nts
rm last.nts
rm PE0.log

#source /home/gempak/GEMPAK5.11.4/Gemenviron
logfile=PE0.log

################################################################################
#
# PE0.csh
#
# Programmers:    Patrick Market and Amanda Cooley
#                 University of Missouri, Atmospheric Science
#
# Written:        01 June 2011
# First modified: 07 June 2011
# Last Edited:    06 November 2016
#
# Short program to interpolate heights in the mid-troposphere in NARR
# grid filesi to support 50-mb integrations.
#
# (c) 2017 FM Software  "Because if it works, it's FM!"
################################################################################

#-------------------------------------------------------
# Designate filename,levels,date,and time to be calculated
#-------------------------------------------------------

times="92110200_ 92110203_ 92110206_ 92110209_ 92110212_ 92110215_
92110218_ 92110221_"

for j in $times
do

time=`expr $j`

dt=`expr $time : '\(......\)'`
gdat=`expr $time : '......\(..\)'`

file="19${time}narr221.gem"
```

```
#-------------------------------------------------------------------
# Interpolate to get HGHT for a few layers in the mid-troposphere
#-------------------------------------------------------------------

$GEMEXE/gdvint<<EOF>> $logfile

GDFILE   = $file
GDOUTF   = $file
GDATTIM  = $dt/${gdat}00F00
GVCORD   = pres/pres
GLEVEL   = 675;625;575;525;475;425;375;325
GPACK    = none

r

EOF

$GEMEXE/gpend

done
```

:::::::
**PE1.csh**
:::::::

```
#!/bin/sh

# Get standard settings
LD_LIBRARY_PATH=/opt/SUNWspro/lib:/usr/X11R6/lib:/usr/lib
export LD_LIBRARY_PATH

rm gemglb.nts
rm last.nts
rm PE1.log

#source /home/gempak/GEMPAK5.11.4/Gemenviron
logfile=PE1.log

###############################################################################
#
# PE1.csh
#
# Programmers:    Patrick Market and Amanda Cooley
#                 University of Missouri, Atmospheric Science
#
# Written:        01 June 2011
# First modified:
# Edited:         24 June 2011, to clean up and finalize.
#                 06 Nov  2016, keep banging away...
#
# This script calculates the moisture flux divergence following
# Doswell et al. (1996), and in this form, forgoes the option
# (for now) to integrate it for each grid element volume (dx dy dz);
# it is renamed as 'sdiv1'.   Integration takes place in a later
# script.
###############################################################################

#-------------------------------------------------------------
# Designate filename,levels,date,and time to be calculated
#-------------------------------------------------------------

pressure="950 900 850 800 750 700 650 600 550 500 450 400 350 300"

times="92110200_ 92110203_ 92110206_ 92110209_ 92110212_ 92110215_
92110218_ 92110221_"


for j in $times
do

time=`expr $j`

dt=`expr $time : '\(......\)'`
gdat=`expr $time : '......\(..\)'`
```

```
file="19${time}narr221.gem"

#---------------------------------------------------------------------
# Calculate Moisture Flux Divergence across grid domain at all levels.
# This operation yields 'sdiva'.
#---------------------------------------------------------------------

for k in $pressure
do

level=`expr $k`
ltop=`expr $k - 25`
lbot=`expr $k + 25`

$GEMEXE/gddiag<<EOF>> $logfile

GDFILE   = $file
GDOUTF   = $file
GDATTIM  = $dt/${gdat}00F00
GFUNC    = mul(-1.0, sdiv(mul(dden($level, tmpc), mixr),obs))
GLEVEL   = $level
GRDNAM   = sdiva
GPACK    = none

r

EOF

$GEMEXE/gpend

#---------------------------------------------------------------------
# Spatially integrate the Moisture Flux Divergence across grid domain
# at all levels.  This operation yields 'sdivt' which is the spatially
# integrated moisture flux divergence for each grid element cube down
# to 1000 mb.
#---------------------------------------------------------------------
#
#$GEMEXE/gddiag<<EOF>> $logfile
#
#GDFILE   = $file
#GDOUTF   = $file
#GDATTIM  = $dt/${gdat}00F00
#GFUNC=mul(1,mul(1,mul(mul(mul(sdiva,32000.0),32000.0),sub(hght@$ltop,hght
@$lbot))))
#GLEVEL   = $level
#GRDNAM   = sdivt
#GPACK    = none
#
#r
#
#EOF
#
#$GEMEXE/gpend
#
```

```
#-------------------------------------------------------------------------
# This operation renames 'sdiva' to 'sdiv1' which is still the
# integrated moisture flux divergence for each grid point
# down to 1000 mb.
#-------------------------------------------------------------------------

$GEMEXE/gddiag<<EOF>> $logfile

GDFILE   = $file
GDOUTF   = $file
GDATTIM  = $dt/${gdat}00F00
GFUNC    = mul(sdiva, 1.0)
GLEVEL   = $level
GRDNAM   = sdiv1
GPACK    = none

r

EOF

$GEMEXE/gpend

done
done
```

:::::::
**PE2.csh**
:::::::

```
#!/bin/sh

# Get standard settings
LD_LIBRARY_PATH=/opt/SUNWspro/lib:/usr/X11R6/lib:/usr/lib
export LD_LIBRARY_PATH

rm gemglb.nts
rm last.nts
rm PE2.log

#source /home/gempak/GEMPAK5.11.4/Gemenviron
logfile=PE2.log

###############################################################################
#
# PE2.csh
#
# Programmers:    Patrick Market and Amanda Cooley
#                 University of Missouri
#                 Atmospheric Science
# Written:        01 June 2011
# Edited:         24 June 2011, to clean up and finalize.
#                 06 November 2016
#
# This script masks out all level non-atmospheric grid levels that
# were actually below the real model surface, and for which no real
# data were observed.
###############################################################################

#-------------------------------------------------------------
# Designate filename,levels,date,and time to be calculated
#-------------------------------------------------------------

pressure="950 900 850 800 750 700 650 600 550 500 450 400 350 300"

times="92110200_ 92110203_ 92110206_ 92110209_ 92110212_ 92110215_
92110218_ 92110221_"


for j in $times
do

time=`expr $j`

dt=`expr $time : '\(......\)'`
gdat=`expr $time : '......\(..\)'`

file="19${time}narr221.gem"
```

```
for k in $pressure
do

level=`expr $k`
ltop=`expr $k - 25`
lbot=`expr $k + 25`

#--------------------------------------------------------------------
# Mask the Moisture Flux Divergence across grid domain for all levels
# where the surface pressure is less than that of the level where
# 'sdiv1' was calculated.  This yields 'sdiv2'.
#--------------------------------------------------------------------

$GEMEXE/gddiag<<EOF>> $logfile

GDFILE   = $file
GDOUTF   = $file
GDATTIM  = $dt/${gdat}00F00
GVCORD   = pres
GFUNC    = mul(sdiv1, lt($lbot, pres@0%none))
GLEVEL   = $level
GRDNAM   = sdiv2
GPACK    = none

r

EOF

$GEMEXE/gpend

done
done
```

```
:::::::
PE3.csh
:::::::

#!/bin/sh

# Get standard settings
LD_LIBRARY_PATH=/opt/SUNWspro/lib:/usr/X11R6/lib:/usr/lib
export LD_LIBRARY_PATH

rm gemglb.nts
rm last.nts
rm PE3.log

#source /home/gempak/GEMPAK5.11.4/Gemenviron
logfile=PE3.log

################################################################################
#
# PE3.csh
#
# Programmers:    Patrick Market and Amanda Cooley
#                 University of Missouri
#                 Atmospheric Science
# Written:        01 June 2011
# Edited:         24 June 2011, to clean up and finalize.
#                 06 November 2016
#
# This script now sums up each column with real integrated moisture
# flux divergence values through 300 mb.  These values then get
# assigned  to GVCORD = none, and GLEVEL = 0.
################################################################################

#---------------------------------------------------------
# Designate filename,levels,date,and time to be calculated
#---------------------------------------------------------

pressure="950 900 850 800 750 700 650 600 550 500 450 400 350"

times="92110200_ 92110203_ 92110206_ 92110209_ 92110212_ 92110215_
92110218_ 92110221_"


for j in $times
do

time=`expr $j`

dt=`expr $time : '\(......\)'`
gdat=`expr $time : '......\(..\)'`

file="19${time}narr221.gem"

for k in $pressure
```

```
do

level=`expr $k`
levelup=`expr $k - 50`

#---------------------------------------------------------------------
# Sum the values for 'sdiv2' from the bottom up.
#---------------------------------------------------------------------

$GEMEXE/gddiag<<EOF>> $logfile

GDFILE   = $file
GDOUTF   = $file
GDATTIM  = $dt/${gdat}00F00
GVCORD   = pres
GFUNC    = mul(1, mul(1, add(sdiv2@$level, sdiv2@$levelup)))
GLEVEL   = $levelup
GRDNAM   = sdiv3
GPACK    = none

r

EOF

$GEMEXE/gpend

done

#---------------------------------------------------------------------
# Assign the summed values for 'sdiv3' @ 300 mb to
# glevel=0, gvcord=none.
#---------------------------------------------------------------------

$GEMEXE/gddiag<<EOF>> $logfile

GDFILE   = $file
GDOUTF   = $file
GDATTIM  = $dt/${gdat}00F00
GFUNC    = mul(1, mul(1, mul(sdiv3@300%pres, 1.000))
GVCORD   = none
GLEVEL   = 0
GRDNAM   = mi0
GPACK    = none

r

EOF

$GEMEXE/gpend

done
```

:::::::
**PE4.csh**
:::::::

```
#!/bin/sh

# Get standard settings
LD_LIBRARY_PATH=/opt/SUNWspro/lib:/usr/X11R6/lib:/usr/lib
export LD_LIBRARY_PATH

rm gemglb.nts
rm last.nts
rm PE4.log

#source /home/gempak/GEMPAK5.11.4/Gemenviron
logfile=PE4.log

###############################################################################
#
# PE4.csh
#
# Programmers:    Patrick Market and Amanda Cooley
#                 University of Missouri
#                 Atmospheric Science
# Written:        01 June 2011
# Edited:         24 June 2011, to clean up and finalize.
#                 06 November 2016
#
# This script converts the accumulated, 3-hour precipitation into
# a mass in Kg for direct comparison to the m_i values calculated
# in the previous scripts, PE0.csh through PE3.csh   .
###############################################################################

#-------------------------------------------------------------
# Designate filename,levels,date,and time to be calculated
#-------------------------------------------------------------

times="92110200_ 92110203_ 92110206_ 92110209_ 92110212_ 92110215_
92110218_ 92110221_"


for j in $times
do

time=`expr $j`

dt=`expr $time : '\(......\)'`
gdat=`expr $time : '......\(..\)'`

file="19${time}narr221.gem"
```

```
#-------------------------------------------------------------------------
# This passage converts the accumulated, 3-hour precipitation values
# from units of  mm  , which is the same as  Kg / m**2.0  ,  to Kg.
#-------------------------------------------------------------------------

$GEMEXE/gddiag<<EOF>> $logfile

GDFILE   = $file
GDOUTF   = $file
GDATTIM  = $dt/${gdat}00F003
GFUNC    = p03m
GVCORD   = none
GLEVEL   = 0
GRDNAM   = mp0
GPACK    = none

r

EOF

$GEMEXE/gpend

done
```

In this GEMPAK  .nts  file, the moisture flux divergence is multiplied by 32 km**2 (1024000000 m**2) to achieve integration over dx and dy.  This operation yields a mass per unit area, as was created for precipitation (mp0) in script PE4.csh.

mp0 is a 3-hour accumulated value, and is effectively a time-integrated value.

mi0 is NOT integrated over 3 hours (multiplied by 10800 sec). Doing so would yield a value with correct units, and perfect cancellation, but also yields values that are otherwise fine, just several orders of magnitude too small.

::::::::
**last.nts**
::::::::

```
GDATTIM 921102/0000F003
GLEVEL  0
GVCORD  none
GFUNC   savs(quo(mp0, mul(mi0^f0000, 1024000000.0)))
GDFILE  1992110200_narr221.gem
CINT
LINE    2/2/2
MAP     1
MSCALE  0
TITLE   1/-2
DEVICE  xw
PROJ    MER
GAREA   #38;-90;5;10
CLEAR   yes
PANEL   0
TEXT    1
SCALE   0
LATLON
CONTUR  0
SKIP    0
FINT    0
FLINE   10-20
CTYPE   C
LUTFIL
STNPLT
```